Evidence for Highly Dispersive Primary Charge Separation Kinetics and Gross Heterogeneity in the Isolated PS II Reaction Center of Green Plants†

ARTICLE *in* THE JOURNAL OF PHYSICAL CHEMISTRY B · MAY 2004

Impact Factor: 3.3 · DOI: 10.1021/jp049562l

5 AUTHORS, INCLUDING:

Ryszard Jankowiak
Kansas State University
193 PUBLICATIONS **4,758** CITATIONS
SEE PROFILE

Valter Zazubovich
Concordia University Montreal
43 PUBLICATIONS **714** CITATIONS
SEE PROFILE

Evidence for Highly Dispersive Primary Charge Separation Kinetics and Gross Heterogeneity in the Isolated PS II Reaction Center of Green Plants†

K. Riley,‡ R. Jankowiak,‡ M. Rätsep,§ G. J. Small,‡ and V. Zazubovich*,‡

Ames Laboratory, USDOE and Department of Chemistry, Iowa State University, Ames, Iowa 50011, and Institute of Physics, University of Tartu, 142 Riia Street, 51014 Tartu, Estonia

Received: January 30, 2004; In Final Form: March 15, 2004

Despite the availability of an X-ray structure and many spectroscopic studies, important issues related to structural heterogeneity, excitonic structure, primary charge separation (CS), and excitation energy transfer dynamics of the isolated reaction center (RC) of photosystem II (PS II) remain unresolved. The issues addressed here include (1) whether the primary CS kinetics at low temperatures are highly dispersive (due to structural heterogeneity), as proposed by Prokhorenko and Holzwarth (*J. Phys. Chem. B* **2000**, *104*, 11563), and (2) the nature of the weak lowest-energy Q_y absorption band at ~684 nm that appears as a shoulder on the intense primary electron donor band (P680). Results of low-temperature nonphotochemical hole burning (NPHB) and triplet bottleneck hole burning (TBHB) spectroscopic experiments (including effects of pressure and external electric (Stark) fields) are presented for the RC from spinach with one of the two peripheral chlorophylls removed. Both NPHB and TBHB are observed with excitations within the P680 and 684 nm bands. Both types of hole spectra exhibit a weak dependence on the burn wavelength (λ_B) between 680 and 686 nm. Furthermore, the permanent dipole moment change ($f\,\Delta\mu$), as determined by Stark-NPHB spectroscopy, is identical (0.9 ± 0.1 D) for the two bands, as are the linear electron−phonon coupling parameters (Huang−Rhys factors $S_{17} = 0.7$ and $S_{80} = 0.2$ for 17 and 80 cm^{-1} phonons). These similarities, together with published fluorescence line narrowed spectra lead us to favor the gross heterogeneity model in which the 684 nm band is the primary electron donor band (P684) of a subset of RCs that may be more intact than P680-type RCs. It is concluded, based also on the linear pressure shift rates for the P680 and 684 nm bands, that population of either P680* (* ≡ Q_y state) or P684* results in both TBHB (due to charge recombination of the primary radical ion pair) and NPHB. It was found that the values of parameters (e.g., electron−phonon coupling, site distribution function) used to simulate the NPHB spectra also provided reasonable fits to the TBHB spectra. Acceptable theoretical simulations of the line-narrowed TBHB spectra were not possible using a single primary CS time. However, satisfactory fits (including λ_B and burn intensity dependences) were achieved using a distribution of CS times. The observed TBHB is due to P680- and P684-type RCs with the faster CS kinetics since the persistent nonphotochemical holes were saturated prior to measuring the TBHB spectra. (RCs exhibiting the most efficient NPHB have slower CS kinetics as well as higher fluorescence quantum yields.) For the TBHB spectra, the same distribution (Weibull) was used for the P680- and P684-type RCs. The distribution describes quite well the distribution of Prokhorenko and Holzwarth for CS times shorter than 25 ps. Finally, the data indicate that electron exchange contributes only weakly (relative to electrostatics) to the inter-pigment excitonic interactions.

1. Introduction

Since its isolation in 1987,[1] the $Q_y(S_1)$ excitonic structure, excitation energy transfer, and charge separation dynamics of the photosystem II (PS II) reaction center (RC) have been the subjects of intense study (as reviewed in ref 2). The recently determined X-ray structure (3.8 Å resolution) of the PS II RC[3] has stimulated greater activity and confirmed that the structural arrangement of the core chlorins (Figure 1) is similar to that of the bacterial RC. P_1, P_2, Chl_1, and Chl_2 are chlorophyll *a* molecules and $Pheo_1$ and $Pheo_2$ are pheophytin *a* molecules. The subscripts denote the polypeptides to which the chlorins are bound, D_1 and D_2, which are analogous to the L and M polypeptides of the bacterial RC. P_1 and P_2, for example, are the structural counterparts of PL and PM (bacteriochlorophyll molecules) of the bacterial RC, the special pair. It is the lowest excited state of the special pair of the bacterial RC that serves as its primary electron donor state (see ref 4 for a review). The X-ray structure also located the two peripheral Chl *a* molecules, Chl_{Z_1} and Chl_{Z_2}, that are bound to D_1 and D_2.[3] In what follows, the RC with 6 Chl *a* molecules will be referred to as RC-6. The RC with one of the two peripheral Chls removed[5] will be referred to as RC-5. Because of their peripheral locations, Chl_{Z_1} and Chl_{Z_2} are not expected to have a significant effect on the Q_y excitonic structure of the core chlorins.[6]

Despite the availability of an X-ray structure and an earlier structural model,[7] several important issues related to excitonic structure and dynamics have yet to be resolved.[2] To a considerable extent, this is due to the severe spectral congestion of the $S_0 \rightarrow Q_y$ absorption spectrum that spans a range of only ~500

† Part of the special issue "Gerald Small Festschrift".

* To whom correspondence should be addressed. E-mail: valterz@iastate.edu.

‡ Iowa State University.

§ University of Tartu.

10.1021/jp049562l CCC: $27.50
Published on Web 05/18/2004

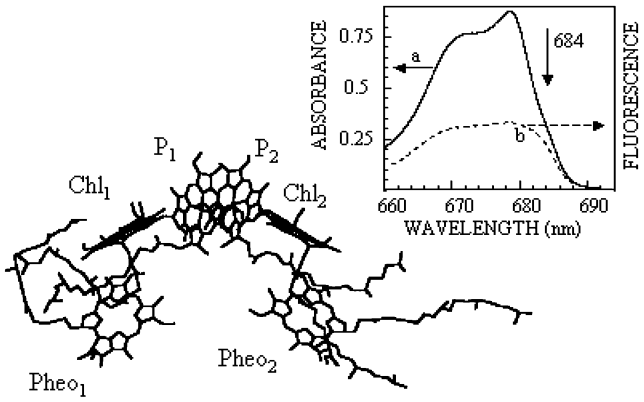

Figure 1. Structure of the isolated PS−II RC (peripheral chlorophylls not shown). Insert: Absorption (a; solid line) and fluorescence excitation (b; dashed line) spectra of PS II RC-5 sample at 5 K. Both spectra are measured in the same experiment and with the same sample. Vertical arrow indicates the shoulder at ∼684 nm.

cm^{-1}, Figure 1. It is generally agreed, however, that the primary electron donor of the isolated PS II RC, P680, contributes significantly to the 680 nm absorption band.

The main issues to be addressed in this paper are the effects of structural heterogeneity on (1) the excitonic composition of the primary electron donor state (P680*) and (2) the primary charge separation kinetics, as well as (3) the nature of the relatively weak absorption shoulder at ∼684 nm indicated by the arrow in Figure 1 for RC-5. Such absorption also exists in RC-6, vide infra.

In early works, it was assumed, by analogy with the bacterial RC, that P_1 and P_2 form a special pair whose lowest excited dimer state is P680*, the primary electron donor state. This assumption was called into question by Tetenkin et al.[8] and later by Durrant et al.,[6] who introduced the so-called multimer (excitonic) model for the six core chlorins. The RC structure used was based on that of the bacterial RC but with the P_1-P_2 distance (Mg...Mg) set at 10 Å, rather than the value of 7.6 Å for P_L-P_M. The calculations took into account diagonal energy disorder; coupling energies were calculated using the point dipole−dipole approximation. It was found that the Q_y states are delocalized over ∼3 chlorins, mainly on either the D_1 or D_2 branch. Thus, a lowest energy, primary donor state highly localized on P_1 and P_2 did not emerge from the calculations. Calculations of a similar vein, but based on the model structure of Svensson et al.[7] and/or the X-ray structure[3] were performed later.[9] The results for the two structures were similar, with the Q_y states mainly delocalized over ∼3−4 chlorins. However, it was *not* found that the states are mainly delocalized over either the D_1 or D_2 branches, consistent with the results of ref 10. Significantly improved fitting of hole-burned and other spectra was achieved with $Pheo_2$ decoupled from the other five chlorins. It was found that the two lowest Q_y states are the most strongly absorbing with the absorption strength of the lowest equivalent to 2.3 Chl *a* molecules and that of the adjacent state equivalent to 1.1 Chl *a* molecules. The calculated splitting between these two states is ∼90 cm^{-1}. A key point for consideration of the 684 nm absorbing chlorin molecule is that all calculations to date do not predict a lowest energy state that is weakly absorbing. Concerning the composition of the lowest energy state, P680*, it was found that, on average, P_1 and P_2 make the largest contributions although the contributions from Chl_1, $Pheo_1$, and, to a lesser extent, Chl_2 are significant.[9] Compositional analysis of the lowest energy state of single complexes revealed that its excitonic composition varies significantly from complex to complex. This provides support for the conclusion of Prokhorenko and Holzwarth[11] that the primary charge separation kinetics at low temperatures are highly dispersive. It should be noted that a recent refinement of the X-ray structure has led to a P_1-P_2 distance of 8.6 Å,[12] 1.4 Å shorter than the value reported in ref 3 and used in ref 9. This distance may be short enough for the electron exchange coupling to be significant.

Concerning the primary charge separation rate at or near room temperature for RC-6, values of $(0.4\ ps)^{-1}$,[13] $(3\ ps)^{-1}$,[14−17] $(8\ ps)^{-1}$,[18] and $(21\ ps)^{-1}$ [19] have been reported. At liquid helium temperatures several groups have reported values in the $(2\text{-}5\ ps)^{-1}$ range.[13,20−25] (The results in ref 25 led to the conclusion that the primary charge separation rate of RC-6 and RC-5 in the low temperature limit are very similar.) However, Prokhorenko and Holzwarth recently reported photon echo data obtained at 1.3 K which, on the basis of theoretical simulations, indicate that there is not a well-defined primary charge separation rate, i.e., the kinetics of primary charge separation are highly dispersive, with charge separation times ranging from a couple of ps to several ns. The dispersive kinetics would be a consequence of the structural heterogeneity leading to a lower energy Q_y state whose chlorin composition varies significantly from RC to RC. Of relevance to this paper is that the simulations of the triplet bottleneck hole burned (TBHB) spectra of P680 presented in ref 25 assumed that the primary charge separation kinetics are nondispersive.

Concerning the weak 684 nm absorption band, it was suggested early on that it corresponds to the lowest energy band of the special pair (P_1,P_2) with the higher energy and more strongly absorbing dimer level located at 680 nm.[26] The same group later argued against that interpretation.[27] It was reported in ref 21 that the 684 nm absorbing chlorin(s) is fragile, e.g., easily disrupted by the detergent TX-100 at concentrations of TX-100 too low to significantly affect the P680 band. It was also observed that the intensity of the 684 nm absorbing chlorin varied in different samples. These observations led to the suggestion that the 684 nm absorbing Chl(s) is a solvent exposed "linker" pigment that may serve to shuttle excitation energy from the proximal antenna complexes to the RC at biological temperatures. The "linker" was later assigned to one of the two peripheral Chl molecules.[28]

New insights on the 684 nm absorbing pigment(s) emerged from the experiments of Völker and co-workers.[29,30] Based on zero-phonon hole (ZPH) action spectra, they determined that the width of the site (state) excitation frequency distribution function (SDF) of the 684 nm absorbing Chl is ∼140 cm^{-1} and ∼150 cm^{-1} for RC-6 and RC-5, respectively, with the gaussian SDF centered near 684 nm. These widths represent static inhomogeneous broadening. Very narrow (≲1 GHz) ZPH widths were observed ($T \leq 4.2$ K) and convincingly attributed to pure dephasing from electron-two level system coupling. Thus, the excitation energy transfer and/or primary charge separation times must be very long (ns time scale) for the 684 nm Chl probed by persistent hole burning. For that reason, the 684 nm state was referred to as a trap state.[30] It has been suggested that this state may be due to a subset of the RCs for which primary charge separation is highly forbidden on energetic grounds.[2] Since such a model does not predict a distinct 684 nm absorption band, the same group proposed that the 684 nm band is the origin band of the primary donor state with the 680 nm band corresponding to a phononic transition involving a ∼80 cm^{-1} mode.[31] Another interpretation put forth is that the 684 nm absorption band is due to the primary donor P684 of intact RC

and that the procedure used to obtain the isolated RC results in structural changes that blue-shift the primary donor band of the majority of the RC to 680 nm. Very recently, Smith et al.[32] reported magnetic circular dichroism spectra (1.7 K) for the O_2-evolving PS II complex from spinach and assigned a narrow ($\sim$45 cm^{-1}) spectral feature at 683.5 nm to the primary electron donor (P684).

We present the results of persistent nonphotochemical hole burning (NPHB) and TBHB experiments designed to provide new insights on primary charge separation and the 684 nm absorbing Chl *a*. High pressure and external electric (Stark) fields are combined with hole burning to enhance spectroscopic selectivity. The experimental data and theoretical simulations are consistent with a model in which gross heterogeneity leads to two types of RC, one in which the primary electron donor absorbs at $\sim$680 nm (P680) and the other at $\sim$684 nm (P684). Intrinsic structural heterogeneity in each type of RC leads to highly dispersive primary charge separation kinetics. The model suggests that the lowest energy Q_y state of RCs (of both types) with the slowest charge separation is the trap state referred to above. Potential problems with the model are considered as well as alternative explanations of the data.

2. Experimental Section

PS II RC-5 complexes containing $\sim$5.3 Chl *a* molecules per two Pheo *a* molecules were prepared and purified from market spinach as described in ref 18. Samples were dissolved in a mixture of MES buffer (pH = 6.5) containing 2 mM dodecyl-maltoside and 5 mM imidizole. Glycerol was added (v/v ratio of 1:2) to ensure formation of high optical quality glasses upon cooling to liquid helium temperatures. Moderate resolution (0.5 cm^{-1}) absorption and hole burned spectra were measured with a Bruker HR120 FT spectrometer. The burn laser was a Coherent 699 ring dye laser with the intra-cavity assembly (ICA) removed (2 GHz line width). This setup was used in some Stark (external electric field) experiments and all high-pressure experiments.

Persistent zero-phonon hole (ZPH) action spectra[33] were obtained with the ICA installed (long term laser line width <20 MHz). Action spectra were obtained in both the transmission and fluorescence detection modes. For the former, light transmitted through the sample was detected with a diode assembly based on a UDT-10 DPI photodiode, optimized for high sensitivity and slow response. For the latter mode, fluorescence was detected by a Hamamatsu 2949 PMT at 90° relative to the excitation beam direction. A 730 nm cutoff filter was used to suppress scattered laser light. Spectra were corrected for the transmission characteristics of the neutral density filters (LOMO, Russia). Spectra obtained in the excitation mode with different filter sets were essentially identical after correction. ZPH were well-fitted with Lorentzian profiles. Fractional hole depths were calculated as the ratio of ΔOD at the peak of ZPH divided by OD prior to burning (transmission mode). For the fluorescence detection mode, the fractional hole depth was calculated as the fluorescence intensity decrease after burning divided by the intensity prior to burning.

Triplet bottleneck hole burned (TBHB) spectra were obtained following saturation of the persistent nonphotochemical hole (NPHB) spectrum, as described in ref 25. This procedure ensures that TBHB spectra correspond to RCs undergoing efficient primary charge separation. The Stark hole burning apparatus is described in ref 34. The setup allows for determination of the response of the ZPH with laser polarization parallel and perpendicular to the applied field. For 665 nm $\leq \lambda_B \leq$ 679 nm, a spectral resolution of 0.5 cm^{-1} was used, vide supra. Burn fluences ranged from $\sim$10 to $\sim$75 J/cm^2. For $\lambda_B \geq$ 680 nm, holes were burned and read with a resolution of 20 MHz (fluorescence excitation mode). In this mode, a burn fluence of 1.5 mJ/cm^2 was used. The high-pressure apparatus used is described in ref 35. When the desired pressure exceeded the pressure of helium solidification at the temperature of the hole burning experiment ($\sim$6 K), the cell was pressurized at $\sim$60 K and then cooled to 6 K.

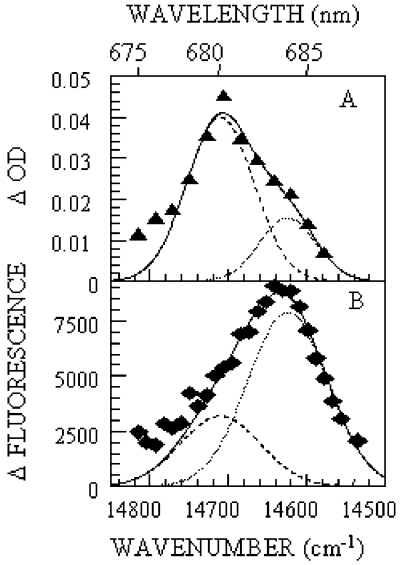

Figure 2. Action spectra obtained in transmission (A; triangles) and fluorescence excitation (B; diamonds) modes with 3 mJ/cm^2 irradiation. Frame A: The best parameters for two-gaussian fit are (peak position/width): 679.9 nm/110 cm^{-1} (dashed line) and 683.9 nm/90 cm^{-1} (dotted line) with the amplitude ratio 2.4:1. Frame B: The best fit parameters are 680.0 nm/120 cm^{-1} (dashed line) and 683.9 nm/110 cm^{-1} (dotted line) with the amplitude ratio of 1:2.4. Solid curves are sums of dashed and dotted curves.

3. Results

Absorbance, Excitation and ZPH Action Spectra. Absorbance (A) and fluorescence excitation (B) spectra for the Q_y region of RC-5 are shown in the insert of Figure 1. The absorption spectrum, with a maximum at $\sim$679 nm and shoulder at $\sim$684 nm, is very similar to those presented in refs 29, 30, 36, and 37. The fluorescence excitation spectrum differs significantly from the spectra reported by den Hartog et al.[30] The maximum at $\sim$679 nm in Figure 1 is broader and much less pronounced. This difference cannot be attributed to sample degradation since the absorption spectrum was recorded immediately after recording the excitation spectrum. We note that fluorescence excitation spectra obtained without correction for the transmission characteristics of the neutral density filters were quite similar to those of den Hartog et al. The difference between the two spectra in Figure 1 establishes that the fluorescence quantum yield is not constant as the excitation is tuned across the absorption spectrum. The decrease in fluorescence quantum yield for excitation wavelengths in the vicinity of 680 nm might be expected given that primary charge separation involving P680 occurs on a time scale as short as a few picoseconds. Figure 2 shows persistent ZPH action spectra obtained in the transmission mode (frame A) and fluorescence excitation mode (frame B) with a burn fluence of 3 mJ/cm^2. (The excitation action spectrum obtained with 0.3 mJ/cm^2 was very similar to that in frame B.) The action spectra correlate with the spectra in Figure 1, e.g., the maximum of the spectrum in frame A and of spectrum a

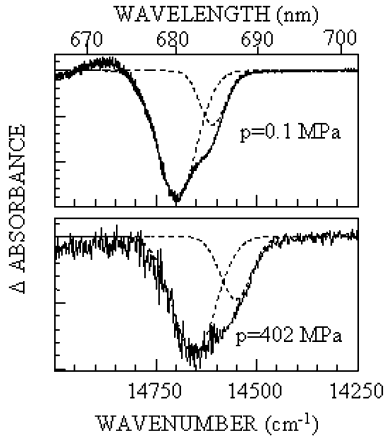

Figure 3. Frame A: Triplet bottleneck hole spectrum resulting from excitation at 665 nm with ~200 mW/cm^2, $p = 0.1$ MPa. The hole is best fitted by a sum of two gaussians (dashed curves), peaked at 14 705 cm^{-1} (680.0 nm) and 14 614 cm^{-1} (684.3 nm). The widths of these gaussians are 115 and 85 cm^{-1}, respectively. Frame B: Triplet bottleneck hole at 402 MPa; the best fit parameters are 14 655/125 and 14 554/90 cm^{-1}.

(absorbance) in Figure 1 are at ~680 nm and both spectra feature a relatively weak shoulder at ~684 nm. The action spectrum in frame A could be well-fitted for $\lambda \geq 676$ nm with two gaussian profiles at 679.9 and 683.9 nm with widths of 110 and 90 cm^{-1}, respectively, and the amplitude of the former (dashed curve) a factor of 2.4 higher than that of the latter (dotted curve). We note that the action spectrum obtained in the transmission mode is very similar to that reported in ref 37, which was obtained with a burn fluence of 15 J/cm^2 and measured with a resolution of 0.5 cm^{-1}. Fitting of the ZPH action spectrum obtained in the fluorescence excitation mode with a single gaussian led to a SDF centered at 683.5 nm with an inhomogeneous width of 130 cm^{-1}, values close to those reported by den Hartog et al.[30] A better fit was obtained by using two gaussians at 679.9 (dashed curve) and 683.9 nm (dotted curve) with the amplitude of the latter a factor of 2.4 higher than that of the former, frame B of Figure 2. This situation is roughly the reverse of that for the action spectrum in frame A of Figure 2.

The results of Figure 2 establish that states absorbing at ~680 and ~684 nm undergo persistent nonphotochemical hole burning (NPHB). Prior to the introduction of the multimer model, it was proposed that[37,38] the state at 680 nm responsible for NPHB is localized on $Pheo_1$ since the nonline narrowed hole profile obtained with nonresonant excitation is very similar to the bleach profile resulting from white light plus dithionite reduction of $Pheo_1$ (primary electron receptor) at 4 K. An additional consideration was that NPHB was not observed for the primary donor absorption band (P870) of the purple bacterium *Rb. sphaeroides*, a consequence of the primary charge separation rate ~(1 ps)$^{-1}$, being several orders of magnitude higher than the NPHB rate. The possibility that P680 → P680* excitation can result in both NPHB and TBHB is considered in section 4.

Pressure Dependent Results. In earlier studies, it was shown that the TBHB spectra of the isolated PS II RC-6 obtained at liquid helium temperatures under nonline narrowing conditions consists of two components centered near 680 and 684 nm.[21] Formation of the triplet state is a result of charge recombination of the radical ion pair associated with primary charge separation. To gain further insight on the two components, nonline narrowed TBHB spectra (6 K) were obtained at pressures of 0.1, 12, 154, 298, and 402 MPa ($\lambda_B = 665$ nm). The 0.1 and 402 MPa spectra are shown in Figure 3, along with fits obtained using two gaussians. At ambient pressure they are centered at 680.0 nm

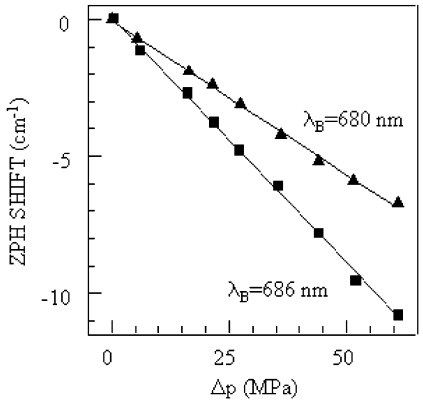

Figure 4. Pressure-induced shifts of the ZPHs burned at 680 nm (triangles) and 686 nm (squares). The shift rates are −0.11 and −0.16 cm^{-1}/MPa, respectively.

(14 705 cm^{-1}) and 684.3 nm (14 614 cm^{-1}), with widths of 115 and 85 cm^{-1}, respectively. Note that these values are very similar to those obtained from the action spectrum in frame A of Figure 2. At 402 MPa, the gaussians are peaked at 14 655 and 14 554 cm^{-1}, with widths of 125 and 90 cm^{-1}. The linear pressure shift rates for the 680 and 684 nm components (states) obtained using the spectra for all five pressures are -0.12 ± 0.01 and -0.15 ± 0.01 cm^{-1}/MPa, respectively. The shift rates of persistent ZPH burned into the 680 and 684 nm bands are, within experimental uncertainty, the same as those given above. The results for λ_B (burn wavelength) = 680 and 686 nm are shown in Figure 4. The respective shift rates are 0.11 ± 0.005 and 0.16 ± 0.01 cm^{-1}/MPa. We emphasize that $\lambda_B = 686$ nm is highly selective for the 684 nm absorbing pigment(s).

Stark Hole-Burning Spectroscopy. Stark hole-burning spectroscopy has proven to be a powerful approach for determining the permanent dipole change ($\Delta\mu$) associated with the $S_0 \rightarrow Q_y(S_1)$ transitions of photosynthetic complexes.[39−41] Typically, one monitors the dependence of the ZPH profile (coincident with λ_B) with the laser polarization parallel and perpendicular to the applied electric (Stark) field. In the absence of splitting of the ZPH in either polarization, $\Delta\mu$ is obtained from the dependence of the ZPH width (Γ) on the applied field ($\mathbf{E}_S$)[42,43]

$$\Gamma(F) = \Gamma_0(1 + F^2)^{1/2} \quad (1)$$

where Γ_0 is the width (fwhm) of the ZPH at zero applied field and

$$F = 2f \cdot \Delta\mu \mathbf{E}_S/\hbar\Gamma_0 \quad (2)$$

with f the local field correction factor. The unit of Γ is circular frequency. The absence of Stark splitting of the ZPH in both polarizations is expected when the matrix-induced contribution to $\Delta\mu$ dominates the intrinsic contribution of the chromophore and is random in a vectorial sense.[42] Stark hole burning data (2.0 K) were obtained for λ_B values between 665.0 and 686.5 nm. The $f \cdot \Delta\mu$ values, in the unit of Debye (D), are listed in Table 1 for $\mathbf{E}_S$ parallel (||) and perpendicular (⊥) to the laser polarization $\mathbf{E}_l$. Values in italic and Roman were obtained in the fluorescence excitation mode (20 MHz resolution) and transmission mode (0.5 cm^{-1} resolution with FT spectrometer), respectively. Representative Stark ZPH broadening data for λ_B = 680 nm, λ_B = 686 nm and $\mathbf{E}_l$ parallel to $\mathbf{E}_S$ are shown in Figure 5. Again, λ_B = 686 nm is highly selective for the 684 nm absorbing chlorin. The solid and dashed curves are the fits to the data obtained with eq 1.

TABLE 1: Dipole Moment Change $f\cdot\Delta\mu$ at Different Wavelengths[a]

wavelength (nm)	$f\cdot\Delta\mu$ (D), $E_S \| E_l$	$f\cdot\Delta\mu$ (D), $E_s \perp E_l$
665	0.4 ± 0.1	0.4 ± 0.1
668	0.6 ± 0.1	0.6 ± 0.1
671	0.7 ± 0.1	0.6 ± 0.1
673	*b*	0.7 ± 0.1
675	*b*	0.8 ± 0.1
679	1.0 ± 0.1	0.9 ± 0.1
680	*0.91* ± 0.05	*b*
681	0.9 ± 0.1	0.85 ± 0.1
682	*0.91* ± 0.05	*0.81* ± 0.05
683	1.0 ± 0.1	0.8 ± 0.1
684	*0.93* ± 0.05	*0.75* ± 0.05
685	0.9 ± 0.1	*b*
686	*0.93* ± 0.05	0.8 ± 0.1
686.5	0.9 ± 0.1	0.8 ± 0.1

[a] Numbers in Roman and italic obtained in the transmission and fluorescence excitation modes, respectively. [b] Not measured.

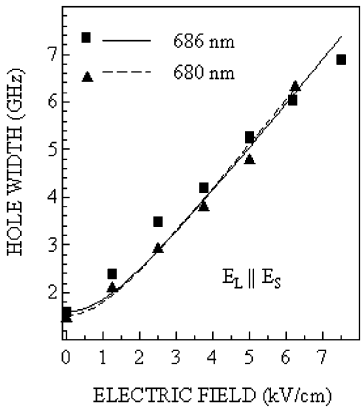

Figure 5. Dependence of the ZPH width on the external electric field for $\lambda_B = 680$ (triangles) and 686 nm (squares). Dashed and solid curves respectively are the fits to the data with eqs 1 and 2. Laser light polarization was parallel to the external field. $f\Delta\mu = 0.9$ D for both wavelengths.

The $f\cdot\Delta\mu$ values in Table 1 are interesting in a couple of respects. First, they are essentially constant ($\sim$0.9 D) for $\lambda_B \gtrsim$ 679 nm, which means that the 680 and 684 nm absorbing states cannot be distinguished on the basis of permanent dipole moment change. Second, $f\cdot\Delta\mu$ values are smaller for $\lambda_B < 679$ nm, and furthermore, $f\cdot\Delta\mu$ values in the range $\sim$0.4$-$0.6 D are typical for a Chl *a* monomer in polymers and in proteins. The small differences ($\sim$10%) between $f\cdot\Delta\mu$ values for $\mathbf{E}_S \perp \mathbf{E}_l$ and $\mathbf{E}_S \| \mathbf{E}_l$ for some of the burn wavelengths may be due to anisotropy of the molecular polarizability and/or the interplay between the molecular, random matrix and nonrandom matrix dipole moment changes.

Dependence of Hole Burned Spectra on Burn Intensity and Burn Wavelength. Persistent NPHB spectra (A$-$D) and transient TBHB spectra (E$-$H) obtained with $\lambda_B = 680$, 682, 684, and 686 nm at 5 K are shown in Figure 6. The burn fluences used to obtain the three spectra in each of frames A$-$D and the burn intensities (IB) used to obtain the four spectra in each of frames E$-$H are given in the caption. The sharpest feature in each spectrum is the ZPH coincident with λ_B. The solid and dashed upward arrows locate the pseudo- and real-phonon sideband holes (PSBH) displaced by 17 cm^{-1} from the ZPH. The spectra in frames A and E are similar to those reported in [25] for RC-6 and $\lambda_B \sim 680$ nm. Of particular importance is that the dependence of the NPHB spectra on λ_B is weak and that the electron$-$phonon coupling of the TBHB spectra would appear to be significantly stronger than that of the NPHB spectra,

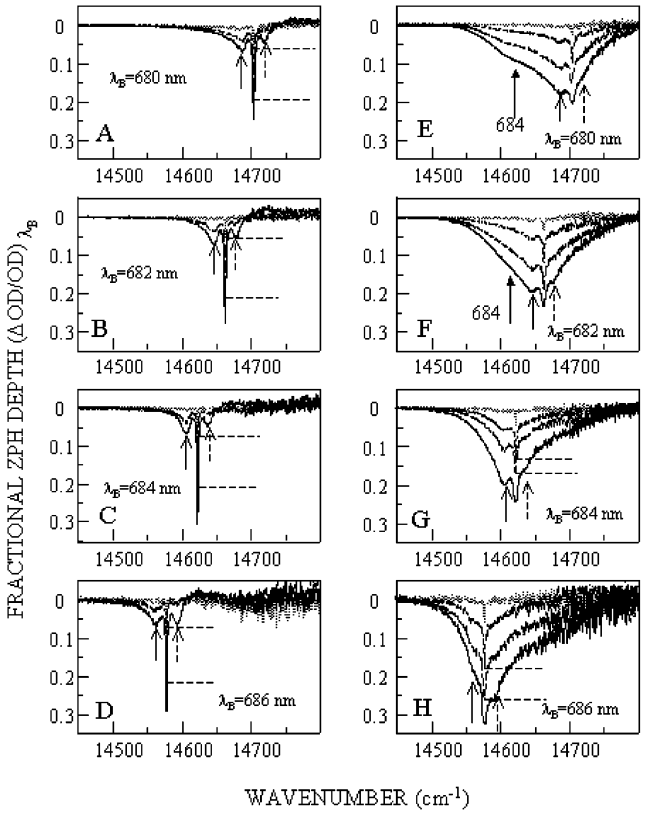

Figure 6. Frames A$-$D: Persistent NPHB spectra for $\lambda_B = 680$, 682, 684, and 686 nm, respectively. Burn fluences are 2.4 J/cm^2 for the dotted curve, 170 J/cm^2 for the dashed curve, and 1600$-$1800 J/cm^2 for the solid curve. Frames E$-$H: Triplet bottleneck hole spectra for $\lambda_B = 680-686$ nm, respectively. Burn intensities are 2, 40, 200, and 600 (at 684$-$686 nm) or 700 (at 680$-$682 nm) mW/cm^2. Vertical solid arrows indicate pseudo-PSBH peaked at 17 cm^{-1} from ZPH. Vertical dashed arrows indicate the real-PSBH. Dashed horizontal lines represent the depths of the ZPH, which are obscured by deeper holes. In frames E and F, the additional solid arrows indicate the broad satellite hole at 684 nm.

as judged by the intensity of the ZPH relative to that of the phonon sideband hole structure. The apparent difference in electron$-$phonon coupling strength has been investigated.[35] For $\lambda_B \sim 680$ nm, the theoretical simulations led to $S_{17} \sim 0.7$ and $S_{17} \sim 1.6$ for the NPHB and TBHB spectra, respectively, where S_{17} is the Huang$-$Rhys factor for the 17 cm^{-1} phonons. In fitting the TBHB spectra it was assumed that the primary charge separation rate is not distributed. That the two values of S_{17} differ significantly was taken as evidence that the chlorin pools (states) responsible for the two types of hole spectra are different. It is shown in section 4 that this need not be the case when the primary charge separation rate is dispersive (distributed).

Hole spectra in Figure 6 were simulated using the theory of Hayes et al.[44] that has been successfully applied to several photosynthetic complexes, including the bacterial RC,[45] the FMO antenna complex,[46] and photosystem I of cyanobacteria.[39,40] The absorption at Ω following burning at ω_B with photon flux P for time τ is given by (low-temperature limit)

$$A_\tau(\Omega) = \exp\left(-\sum_k S_k\right)\prod_k \sum_{R=0}^{\infty}\left(\frac{S_k^R}{R!}\right)\int d\omega G(\omega) e^{-\sigma P\phi\tau L(\omega_B-\omega)} l_{R,k}(\Omega-\omega-R\omega_k) \quad (3)$$

where $G(\omega)$ is the site (or state) energy distribution function

TABLE 2: Parameters Used to Fit Persistent and Triplet Bottleneck Hole Spectra

parameter	686 nm holes	680 nm holes
P684 SDF[a] peak/width	684.7 ± 0.5 nm/90 ± 10 cm^{-1}	
P680 SDF peak/width	680.3 ± 0.5 nm/110 ± 10 cm^{-1}	
peak intensity ratio (P680: P684) ≡ R	2.5:1	
phonon frequency ω_1:	17 ± 1 cm^{-1}	
one-phonon profile (ω_1)[b]	11 ±1 cm^{-1}/16 ± 2 cm^{-1}	
Huang−Rhys factor S_{17}	0.7 ± 0.1	
phonon frequency ω_2:	80 ± 5 cm^{-1}	
one-phonon profile (ω_2)[c]	90 ± 10 cm^{-1}	
Huang−Rhys factor S_{80}	0.2 ± 0.1	
homogeneous ZPL width for persistent holes	0.5 cm^{-1} [d]	1.0 cm^{-1}
homogeneous ZPL width for triplet bottleneck holes	subject to Weibull distribution with α = 1.2 and maximum at 0.6 cm^{-1}.	

[a] SDF ≡ site (state) excitation frequency distribution function. [b] Gaussian shape on low-energy side (fwhm = 11 ± 1 cm^{-1}) and Lorentzian shape on high-energy side (fwhm = 16 ± 2 cm^{-1}). [c] Gaussian with fwhm of 90 ± 10 cm^{-1}. [d] Resolution-limited.

(SDF) of the ZPL, σ is the integrated absorption cross-section, ϕ is the hole burning quantum yield, and S_k and ω_k are the Huang−Rhys factor and frequency of the kth phonon. The $l_{R,k}$ are line shape functions with $R = 0, 1, 2, \ldots$ corresponding to the 0-, 1-, 2-,... phonon transitions. $l_{R=0}$ is the ZPL shape function (a Lorentzian). $L(\omega_B-\omega)$ is the single site absorption spectrum for the ZPL centered at the burn frequency ω_B

$$L(\omega_B-\omega) = \exp(-\sum_k S_k)\prod_k\sum_{R=0}^{\infty}\left(\frac{S_k^R}{R!}\right)l_{R,k}(\omega_B-\omega-R\omega_k) \quad (4)$$

The hole spectrum is the difference between post-burn and pre-burn ($A_0(\Omega)$) spectra

$$A_t(\Omega) - A_0(\Omega) \quad (5)$$

We emphasize that eqs 3 and 5 account for the fluence broadening of the ZPH.

We consider first simulations of the persistent NPHB spectra. Quality of the fits should be based on the ZPH and the pseudo-PSBH since the real-PSBH is interfered with by the anti-hole,[47] which is not accounted for in eq 3. In addition to the 17 cm^{-1} phonons, the 80 cm^{-1} phonons active in the fluorescence line-narrowed (FLN) spectra of the isolated PS II RC[30] were included in the simulations. The first approximations to the one-phonon profiles of the 17 and 80 cm^{-1} phonons could be obtained directly from the FLN spectra. The Huang−Rhys factors S_{17} and S_{80} were adjustable parameters. It was not possible to simultaneously fit the persistent NPHB spectra for the four λ_B values with a SDF that is a single gaussian, but it was possible using a sum of two gaussians, as suggested by the ZPH action spectrum in frame A of Figure 2. All best fit parameter values are listed in Table 2. In frame A of Figure 7, the experimental hole burned spectrum (λ_B = 680.0 nm, burn fluence ~1700 J/cm^2) is compared with three calculated spectra. The best fit (red curve) was obtained with the parameter values in Table 2 (see Figure 7 caption for parameters of other simulated spectra). The experimental hole spectrum for λ_B = 686 nm (burn fluence ~1700 J/cm^2) is shown in frame B of Figure 7. The fit (dashed curve) was obtained with the parameter values in Table 2. As in frame A, the fit to the right of the ZPH is poor because of the neglect of the anti-hole.

Turning next to the TBHB spectra (E−H) of Figure 6, it was also found that significantly improved fits were obtained when a SDF that is the sum of two gaussians was used, consistent with the nonline narrowed TBHB spectra in Figure 3. However, it was not possible to obtain satisfactory fits to spectra for λ_B = 680, 682, 684, and 686 nm and the four burn intensities.

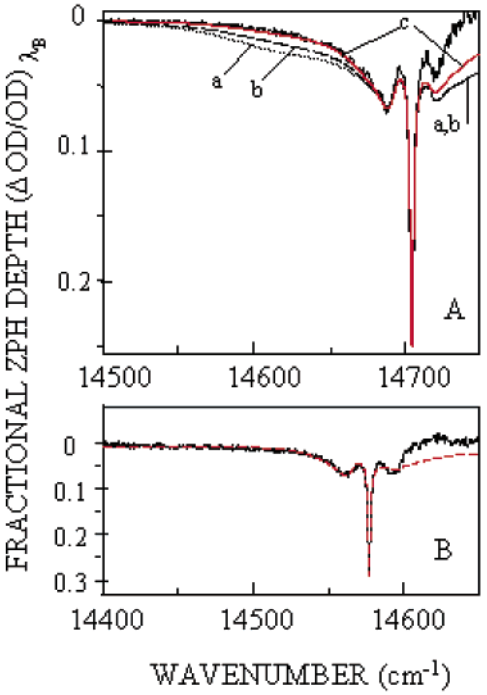

Figure 7. Saturated persistent holes burned at 680 (A) and 686 nm (B), black solid curves, and their fits according to the model by Hayes et al.[45] (see Table 2 for parameters). In frame A dotted (a) and dashed (b) curves are for $S_{17} = S_{80} = 0.7$, the parameters deduced from FLN spectra.[31] Ratio of peak intensities of 680 and 684 nm SDFs was 2.5:1 (a) and 5:1 (b). Red curve corresponds to $S_{17} = 0.7$, $S_{80} = 0.2$ and the SDF peak ratio of 2.5:1. In frame B, only the spectrum calculated with latter parameters is shown (red) along with the experimental spectrum (black).

This is illustrated in frame D of Figure 8 for λ_B = 686 nm and burn intensities of 40, 200, and 600 mW/cm^2. Calculated spectra are shown for S_{17} = 1.25 (blue curve) and 1.50 (red curves); all other parameter values are as given in Table 2 except that the ZPL width was set equal to 2 cm^{-1} and the shape of the one-phonon profile of the 17 cm^{-1} mode changed slightly to improve the fits. The 2 cm^{-1} width corresponds to the primary charge separation time of ~5 ps reported in ref 25, T = 5.0 K. It proved impossible to simulate the peak intensity and width of the ZPH and the intensity and shape of the phonon sideband hole structure using a *fixed* ZPL width. In the following section, it is shown that a distribution of ZPL widths (charge separation rates) results in significantly better fits to the TBHB spectra.

4. Discussion

We begin by considering possible assignments for the 684 nm absorbing chlorin(s). Following that the question of whether

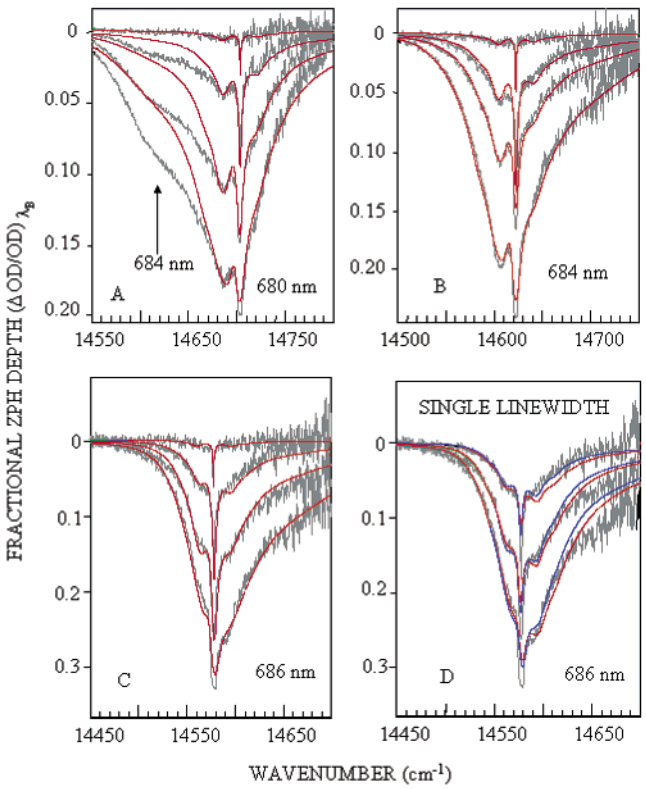

Figure 8. Frames A−C: Experimental (black) and calculated (red) triplet bottleneck hole spectra obtained with the same electron−phonon coupling parameters as used to fit persistent holes ($S_{17} = 0.7$, $S_{80} = 0.2$) and a distribution of homogeneous ZPL widths depicted in Figure 9. (Burn wavelengths are 680, 684, and 686 nm in frames A−C, respectively.) Frame D: The hole spectra for $\lambda_B = 686$ nm and their fits with no ZPL width distribution, fixed ZPL width of 2 cm^{-1} and strong electron−phonon coupling. Blue curve: $S_{17} = 1.25$, red curve: $S_{17} = 1.5$.

the primary charge separation kinetics are highly dispersive is addressed or, equivalently, the question of whether the primary electron donor state (lowest energy Q_y state) is well defined. The section ends with some remarks on the strength of the excitonic couplings between the core chlorins.

A. Nature of the 684 nm Absorbing Chlorin. The absorption spectrum in Figure 1 and hole burned spectra in Figures 2, 3, and 6 provide convincing evidence for the existence of the 684 nm absorbing chlorin(s). In view of the multimer model, one might propose that the weak 684 nm band is due to the lowest energy exciton level of the core chlorins. However, the excitonic calculations are inconsistent with this since they predict that the lowest energy Q_y state should be the most strongly absorbing, not weakly absorbing.[6,9,10] Also inconsistent with this are the TBHB spectra shown in frames G and H of Figure 6 obtained with $\lambda_B = 684$ and 686 nm, wavelengths quite highly selective for the 684 nm band. The spectra are devoid of any intense satellite hole structure that lies to higher energy of the hole peaked at λ_B (the spectral region higher in energy than 14 800 cm^{-1} (676 nm), which is not shown in frames G and H, also showed no hole structure). Such satellite hole structure would be a natural consequence of the weak 684 nm band corresponding to the lowest energy Q_y state. A nice example of such satellite hole structure is the special pair of the RC of *Rps. viridis*.[48] It was shown that a hole burned in the lower dimer band (P_) of the special pair produced a satellite hole in the higher energy upper dimer band (P_+).

A second interpretation of the 684 nm band was that it is the origin of the primary electron donor's absorption with the P680 band corresponding to the one-quantum transition of a ∼80 cm^{-1} vibration (phonon).[2] This interpretation is untenable since the absorption spectrum (Figure 1) and TBHB spectra (Figure 3) lead to a Huang−Rhys factor (S_{80}) of ∼2. The Franck−Condon progression for $S_{80} \sim 2$ would exhibit a maximum for the two-quantum transition at 2×80 cm$^{-1} = 160$ cm^{-1}, which is clearly absent in the TBHB spectra of Figure 3. We note also that a lengthy Franck−Condon progression in an 80 cm^{-1} mode is absent in the TBHB spectrum shown in frame H of Figure 6. Also, the observation that the 684 nm band is fragile, whereas the P680 band is much less so is also inconsistent with the above interpretation.

In the absence of gross structural heterogeneity, a more likely assignment for the 684 nm band is that it corresponds to a localized Q_y transition of a particular RC chlorin that lies lower in energy than the primary electron donor's absorption (P680). Such a state would serve as a trap state. Because of the aforementioned fragility, it was proposed that the responsible chlorin is one of the two peripheral Chls.[38] (It is known with certainty that one of the peripheral Chls absorbs near 670 nm[2].) There are, however, potential problems with this assignment. First, the results of the fs pump−probe experiments on RC-5 and RC-6 at room temperature indicate that both peripheral Chls absorb near 670 nm.[5] Second, the Q_y absorption spectrum for RC-5 calculated with either the multimer or pentamer excitonic Hamiltonians for the *core chlorins*, when added to the absorption of the peripheral Chl, does not fit well the observed spectrum unless the latter absorption is located near 670 nm, not 684 nm.[6,9,10] A third (possible) problem is related to motional narrowing of the inhomogeneous broadening of the site (chlorin) Q_y transition due to excitonic delocalization. It was determined in ref 37 that the site inhomogeneous broadening is, on average, ∼200 cm^{-1}. Motional narrowing resulted in reduction of this width to ∼120 cm^{-1} for the observed "delocalized" transitions.[37,9] The observed inhomogeneous width for the 684 nm band is only ∼90 cm^{-1} (Table 2), slightly narrower than the inhomogeneous width of the P680 band which one expects to be motionally narrowed. The 90 cm^{-1} width would seem to be too narrow to be attributed to a transition localized on a single chlorin. This line of reasoning can be used to argue against the 684 nm band being due to a transition localized on any of the core chlorins. Nevertheless, the possibility that the 684 nm band is due to such a localized state cannot be excluded at this time.

Model for the 684 nm Absorbing Chlorin(s) Based On Gross Structural Heterogeneity. In this model, the P680 and 684 nm bands are considered to arise from the same "subset" of pigments. At low temperatures the oxygen-evolving PS II (D_1/D_2-cyt b559 RC plus CP43 and CP47 proximal antenna complexes) of spinach and cyanobacteria exhibits a primary electron donor absorption band near 684 nm (P684)[32,49] rather than 680 nm. The possibility that the biochemical procedure used to isolate and solubilize the RC shifts the P684 nm band of the majority of the *intact* RCs to 680 nm, while leaving a smaller fraction of RCs that still absorb at 684 nm, is worthy of consideration. Removal of the CP43 and CP47 antenna complexes might destabilize the RC, leading to a blue shift of the P684 band. An additional consideration is that the two plastoquinones of the RC are removed during the isolation procedure.[2] This "P680−P684 model" for the isolated RC would appear to be consistent with the observation that the 684 nm absorbing chlorin(s) of the isolated RC are especially fragile. However, our intent is to be more general and explore the possibility that the isolated RC consists of two subpopulations

with primary electron donor absorption bands at 680 nm (P680) and 684 nm (P684), regardless of the origin of heterogeneity.

This possibility is supported by the experimental results presented here. First, those in frames E−H of Figure 6 show that TBHB spectra of comparable intensity result from excitation at 680 and 686 nm, with the latter wavelength selective for the 684 nm state (P684*). Given that triplet state formation is the result of charge recombination of a primary radical ion pair,[20,50] it appears certain that P680* and P684* have in common that they serve as primary electron donor states. Second, the permanent dipole moment change for the $S_0 \rightarrow$ P680* and $S_0 \rightarrow$ P684* transitions are identical within experimental uncertainty, $f \cdot \Delta\mu \sim 0.9$ D, Table 1. Third, the linear pressure rates of -0.12 and -0.15 cm^{-1}/MPa for the 680 and 684 nm absorption bands, respectively, are nearly the same. We note that this shift rate is linearly proportional to the local compressibility κ[42] so that, all other things being equal, a ~20% difference in κ would account for the difference between the two shift rates. Fourth, the fluorescence line narrowed spectra obtained with laser excitation wavelengths between 679 and 686 nm exhibited identical vibronic structures (vibrational frequencies and relative vibronic intensities).[31] This is consistent with the observation that the persistent NPHB spectra in frames A−D of Figure 6 are essentially independent of λ_B. More specifically, the hole spectra can be fitted using the same set of electron−phonon coupling parameter values for both the 680 and 684 nm states (Table 2). Examples are shown in Figure 7 for $\lambda_B =$ 680 and 686 nm.

The above results establish that the properties of the 680 and 684 nm states are very similar. Such similarity would not be expected if the latter state was localized on a single chlorin molecule, whereas P680* is delocalized over P_1 and P_2 and other pigments.[9] One has, therefore, an additional argument against the 684 nm state being localized. On the other hand, the results support the P680−P684 (gross structural heterogeneity) model. In this model, the excitonic compositions of the 680 and 684 nm states are, on average, similar; this despite the 4 nm shift that may be due mainly to nonexcitonic interactions (dispersion, van der Waals, H-bonding).

B. Simulation of Triplet Bottleneck Hole-Burned (TBHB) Spectra with Dispersive Charge Separation Kinetics. The results in Figure 6 show that both persistent NPHB and transient TBHB spectra can be generated throughout the 680 and 684 nm absorption bands. In the first hole burning studies of the isolated PS II RC, in which λ_B was near the maximum of the 680 nm absorption band, the TBHB spectra were assigned to P680*, the primary electron donor state.[20,28] The persistent NPHB was attributed to a Q_y state localized on $Pheo_1$ for reasons given above. As a result, the 680 nm absorption band was proposed to be due mainly to P680 but with a significant contribution from $Pheo_1$, whose absorption is quasidegenerate with that of P680. In view of the hole burned spectra presented here for $\lambda_B = 684$ and 686 nm (Figure 6), one might propose, with the P680−P684 model in mind, the same scenario for the 684 nm absorption band.

Recent results, however, suggest an alternative model in which (for both the 680 and 684 nm bands) the "same" Q_y state is responsible for both NPHB and TBHB. (In this model, the existence of P680 and P684 due to gross heterogeneity is retained.) First, the photon echo data (1.3 K) of Prokhorenko and Holzwarth[11] strongly indicate that the kinetics of primary charge separation are highly dispersive, with time constants ranging from a few nanoseconds to a couple of picoseconds. Even for the most efficient nonphotochemical hole burning systems the rate constant is only ~$(10\ ns)^{-1}$.[51] Thus, with the just mentioned dispersive kinetics for charge separation, the quantum yield for NPHB would vary over several orders of magnitude and the most efficient nonphotochemical hole burning RCs would also have the highest fluorescence quantum yields. We note that Groot et al.[52] reported a fluorescence quantum yield of 0.07 for RC-6. Second, and as pointed out earlier, all calculations on the Q_y excitonic structure of the core chlorins do not predict a transition highly localized on $Pheo_1$.

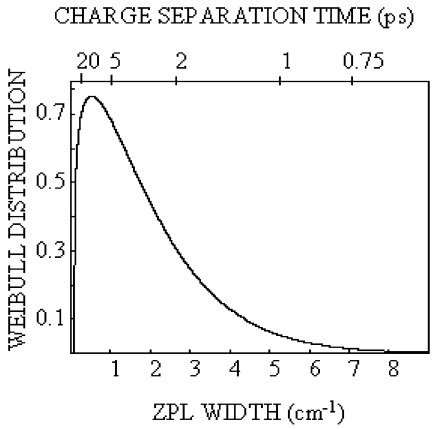

Figure 9. Weibull distribution of the homogeneous ZPL widths used in this work. Distribution is offset along the ZPL width axes by 0.2 cm^{-1} and peaked at 0.6 cm^{-1} (9 ps primary charge separation time).

In using the alternative (new) model to simulate the TBHB spectra in Figure 6, a distribution function that describes the dispersion of charge separation times (or, equivalently, the distribution of zero-phonon line widths; 1 ps $\rightarrow$ 5 cm^{-1}) is required. The Weibull function $W(x) = \alpha x^{\alpha-1} \exp(-x^{\alpha})$ was chosen, in part, because it provides an acceptable description of the shorter charge separation times reported by Prokhorenko and Holzwarth.[11] To reduce the number of free parameters, the value of α was taken to be the same for both the 680 and 684 nm states, which is reasonable within the P680−P684 model. In addition, the electron−phonon coupling parameters for both states were then taken to be the same and independent of burn wavelength. With reference to eqs 3 and 5, the quantum yield for charge separation can be set equal to unity since the TBHB spectra were obtained under conditions which ensure that only RCs with charge separation times much shorter than a few ns (Chl *a* natural radiative lifetime) contribute. Thus, the simulations with eq 5 simply involved allowing for a distribution (Weibull) of widths for the zero-phonon line shape function ($l_{R=0}$ in eq 3). We note that this width is automatically added to the widths of the phonon sideband transitions associated with the 17 and 80 cm^{-1} modes. The relative values of the burn intensities for each burn wavelength were not adjustable parameters; that is, they were determined by the experimental intensities.

The simulated spectra (red curves) are compared against the experimental TBHB spectra in frames A, B, and C of Figure 8 for $\lambda_B = 680$, 684, and 686 nm, respectively. A surprising and interesting finding was that the values of the electron−phonon coupling and SDF parameters (see Table 2) that provide reasonable fits to the persistent NPHB spectra (examples shown in Figure 7) also provide acceptable fits to the TBHB spectra. The Weibull distribution function ($\alpha = 1.2$) that led to these best overall fits is shown in Figure 9. Note that it is offset along the abscissa. The reason for the offset is that the TBHB spectra were obtained after saturating persistent NPHB at λ_B (see section 2). This protocol was originally introduced to eliminate interfer-

ence from NPHB due to $Pheo_1$ to the TBHB spectra of P680.[20] What this means for the model being considered is that the RCs with the slowest charge separation kinetics have been burned away (persistently) and, therefore, do not contribute to the TBHB spectra. The offset was an adjustable parameter; its value in Figure 9 is 0.2 cm^{-1} (25 ps). Thus, only RCs with a charge separation time shorter than ~25 ps contribute to the TBHB spectra.

For all λ_B values, a distribution of ZPL widths gave considerably better fits than a single ZPL width (charge separation time). This can be seen for $\lambda_B = 686$ nm by comparing the spectra in frame C with those in frame D (fixed ZPL width), Figure 8. (The spectra for the lowest burn intensity are not shown in frame D because of very poor agreement between the observed and simulated spectra.) The red and blue curves in frame D were calculated, respectively, with Huang−Rhys factor $S_{17} = 1.5$ and 1.25. The simulated spectra in frame D reveal the problem encountered with all burn wavelengths, namely, that it is impossible to achieve acceptable fits to both the phonon sideband hole (PSBH) structure and the zero-phonon hole (ZPH) when the width of the ZPL is assigned a constant value. The increase in width of the ZPH with increasing burn intensity in the simulated spectra shown in frame D is due to fluence broadening,[53,54] which is accounted for in the hole burning theory used. The fits of the simulated spectra shown in frame C, obtained with a distribution of charge separation times, are clearly superior. Now the increase of ZPH width with increasing burn intensity is due to both fluence broadening and spectral dynamics (the induced absorption rate is inversely proportional to the width of the ZPL which, in turn, is inversely proportional to the primary charge separation time). The agreement between the simulated and experimental spectra obtained with distributed charge separation kinetics and $\lambda_B =$ 684 nm is also quite satisfactory, frame B of Figure 8. This is also the case for $\lambda_B = 680$ nm, frame A. The apparent discrepancies at ~684 nm (also seen for $\lambda_B = 682$ nm, not shown) do not signal a problem with the model. The broad feature near 684 is a satellite hole due to downward energy transfer to the lowest energy exciton level of P684-type RCs following excitation at 680 nm of the second lowest energy exciton level. Such energy transfer is not accounted for in eq 3.

The results in Figures 7 and 8 (and others not shown) establish that the persistent NPHB spectra and TBHB spectra can be understood in terms of the P680−P684 model and a common set of values for the parameters that define the electron−phonon coupling and the SDF for both P680 and P684 provided the charge separation kinetics are taken to be dispersive. Of considerable interest is that in the simulation of the TBHB spectra dispersive charge separation kinetics results in weak electron−phonon coupling ($S_{17} = 0.7$), whereas nondispersive kinetics results in strong coupling ($S_{17} \sim 1.5$). The latter value is similar to those reported earlier.[28,36] In those works, it was assumed that the kinetics are nondispersive. A detailed understanding of how dispersive kinetics results in an "apparent" weakening of the coupling is rather involved because the hole burned spectrum consists of four contributions:[55] the ZPH; the real-PSBH that builds, in a Franck−Condon sense, on the ZPH; the pseudo-PSBH that is the result of "sites" whose ZPLs lie lower in energy than ω_B and which absorb via their phonon sideband. Hole burning ensues following relaxation of the phonons and population of the zero-point level; and the phonon structure that builds on the pseudo-PSBH in a Franck−Condon sense. One should also keep in mind that the ZPHs of RCs with the slowest charge separation kinetics will saturate (reach maximum depth) first since the induced absorption rate is proportional to the charge separation time (or inversely proportional to homogeneous width of the ZPL). Fluence broadening of the ZPH increases rapidly as saturation is approached.[53,54] In the case of single-exponential kinetics, the increase of ZPH width seen in frames E−H of Figure 6, with increasing burn intensity would be due solely to saturation broadening. For a given range of burn intensities (starting at the shallow burn limit), the greater the increase in width, the larger S_{17}. To a reasonable approximation, the Franck−Condon factor for the ZPH is $\exp(-2S_{17})$.[45] Thus, for a given homogeneous width of the ZPH, the burn intensity required to saturate the ZPH decreases with increasing S_{17}. In case of dispersive kinetics, such as described by the Weibull distribution in Figure 9, the ZPH broadening is due to both fluence broadening and spectral dynamics, the latter associated with charge separation kinetics. Thus, correcting the observed broadening for the contribution due to spectral dynamics would lead to less broadening due to fluence broadening and, as a consequence, a lower value of S_{17}. One additional point has to do with the contribution of the ZPH to the spectral "pedestal" region of the real-PSBH and pseudo-PSBH. For a fixed homogeneous width of the Lorentzian ZPH, the larger the ratio of the integrated intensity of the underlying pedestal to that of the ZPH (which is superimposed on the pedestal), the stronger the electron−phonon coupling. Given the Weibull distribution in Figure 9 and the 2 cm^{-1} ZPH width used to fit the TBHB spectra in frame D of Figure 8, it is clear that the contribution to the pedestal in the case of dispersive kinetics would be greater than in the case of nondispersive kinetics, especially at the later stages of hole burning. This would also lead to a lower value of S_{17} in the case of dispersive kinetics.

C. Excitonic Couplings between the Core Chlorins. As discussed in the Introduction, excitonic calculations[6,9,10] based on the X-ray structure of the PS II RC and guided by the observation that the Q_y absorption spectrum spans a range of only ~500 cm^{-1}, as well as an experimental value for the width of the SDF of the core chlorins (~200 cm^{-1}), indicate that the Q_y states of the core cofactors are delocalized over ~3−4 chlorins. This, despite the fact that the strongest pairwise coupling is only ~150 cm^{-1} (between P_1 and P_2). Jankowiak et al.[9] found that several types of optical spectra (low temperature) were best fitted if $Pheo_2$ was decoupled from the other core chlorins (P_1, P_2, Chl_1, Chl_2, and $Pheo_1$). One has, therefore, a "pentamer" model for the Q_y states. Decoupling would require a significant weakening of the interaction between $Pheo_2$ and Chl_2 relative to the interaction between $Pheo_1$ and Chl_1 (see Figure 1). Recently, Frese et al.[56] reported that $f\cdot\Delta\mu$ for the $S_0 \rightarrow Q_x$ transitions of $Pheo_1$ and $Pheo_2$ are very different, 3.0 and 0.6−1.0 D, respectively. The difference is most likely due to the "matrix" induced contribution to $f\cdot\Delta\mu$ on the D_1 side of the RC being much larger than on the D_2 side. Interestingly, the very recently reported X-ray structure (3.7 Å resolution) of PS II from *Thermosynechococcus vulcanus* revealed that the two caroteniod molecules in the RC are located on the D_2 side, quite close to $Pheo_2$.[57] Thus, there are some reasons to speculate that $Pheo_2$ could be decoupled, e.g., dielectric screening might lead to significant weakening of the $Pheo_2$−Chl_2 coupling.

It is worthwhile to compare the low-temperature absorption spectrum of RC-5 calculated with the pentamer Hamiltonian given in [9] with the experimental spectrum. The shorter dashed curve in frame A of Figure 10 is the calculated spectrum for the core chlorins (peripheral Chl not included). The six

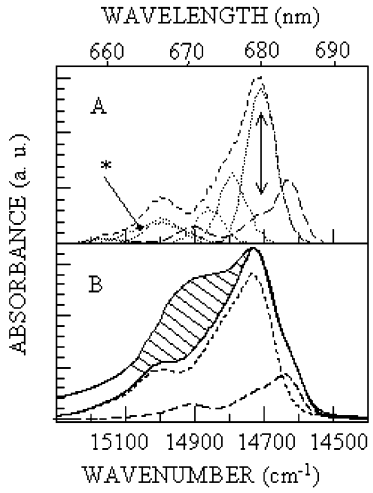

Figure 10. Simulations of absorption spectra. Dotted lines in frame A represent the excitonic states (and the state localized on the decoupled $Pheo_2$ at 668 nm; marked with a slanted arrow with an asterisk) of the pentamer model by Jankowiak et al.[9] neglecting electron−phonon coupling. The short-dashed line is the sum of the dotted curves. The long-dashed line represents the spectrum of the P684-type RCs. Short- and long-dashed curves in frame B are the result of convolution of the respective curves from frame A with the single site spectrum. Thin solid curve is the sum of long- and short-dashed curves. Thick solid curve is the experimental absorption spectrum. Shaded region represents the absorption of the peripheral Chl *a* peaked at ∼670 nm. Vertical arrow in frame A indicates that the lowest state of P680-type RCs and the second-lowest state of P684-type RCs are degenerate.

underlying dotted curves are the absorption bands of the six Q_y states. That of the decoupled $Pheo_2$ is marked by the asterisk and is located at 668 nm with a fwhm of 180 cm^{-1}. The other five bands correspond to the delocalized states. For these states, the SDFs of the five coupled chlorins were centered at 671 nm (fwhm ∼ 180 cm^{-1}),[9] values close to those given in ref 9. With the P680−P684 model in mind, the shorter dashed curve should be viewed as the absorption spectrum of P680-type RCs, less the peripheral Chl. The longer dashed spectrum is that of P684-type RCs, a 4 nm shifted replica of the P680-type spectrum. (Based on the action spectra in Figure 2 and the TBHB spectra in Figure 3, we estimated that the ratio of intensity of the P680 absorption band to that of the 684 nm band is ∼2.5. This leads to the result that the P684-type RCs contribute ∼25% of the total absorption, in reasonable agreement with the spectra in frame A of Figure 2.) The two spectra do not include electron−phonon coupling. We used the electron−phonon coupling parameter values in Table 2 to define a single site absorption spectrum which was convolved with the six inhomogeneously broadened absorption bands of both the P680 and P684 RCs. The resulting (summed) spectra are the short dashed (P680) and long dashed (P684) in frame B of Figure 10. Their sum is the thin solid line spectrum, which should be compared with the experimental spectrum (thick solid line). The fit to lower energy of the maximum of the 680 nm band is satisfactory. The discrepancy to higher energy (hatched area) is most reasonably assigned mainly to the single peripheral Chl (∼670 nm) that was not included in the simulations, i.e., it seems unlikely that the 684 nm absorption band is due to the peripheral Chl. We note that vibronic transitions that build on the origin bands at 680 and 684 nm should make a weak contribution to the absorption at ∼670 nm.

Concerning the pairwise excitonic interactions (electrostatic) of the core chlorins of the PS II RC, we note that, although they are rather small (≲150 cm^{-1}), the Q_y states tend to be delocalized because the larger interactions are comparable in magnitude to the differences between the chlorin site excitation energies, as well as the width of the site excitation energy distribution functions.[8−10] (There is no physical basis for asserting that all of the Q_y states are localized, as Diner and co-workers have.[58]) The question arises as to whether any experimental data indicate that electron-exchange coupling contributes significantly to pairwise interactions (the most likely one being between P_1 and P_2). Such coupling introduces charge-transfer character to the excited states, as reviewed in ref 4. Three indicators for appreciable electron-exchange coupling are the electron−phonon coupling strength, the permanent dipole moment change, and the linear pressure shift of the $S_1(Q_y) \leftarrow S_0$ transitions. These three properties are generally positively correlated (see refs 39 and 40 and references therein). As discussed in those works, the linear pressure rate (R_p) for the $S_1(\pi\pi^*) \leftarrow S_0$ transition frequency is ∼ −0.05 to −0.15 cm^{-1}/MPa for *monomer* chromophores in glasses and polymers at low temperatures, $f\cdot\Delta\mu \sim 0.4-0.6$ D for the Chl *a* monomer in polymers or a localized Q_y state and, finally, the total Huang−Rhys factor (S_t) for low-frequency phonons is most often less than 1 (weak linear electron−phonon coupling). As reviewed in ref 59 for Chl dimers, $|R_p| \gtrsim 0.3$ cm^{-1}/MPa, $f\cdot\Delta\mu \gtrsim 1$ D, and $S_t \gg 1$ (strong coupling) are values which indicate that the monomers are strongly interacting with electron exchange coupling making a significant contribution. Examples of such a Chl *a* dimer state are the red-most antenna state of the cyanobacteria *Synechocystis* PCC 6803 and *Synechococcus elongatus* at 714 and 719 nm, respectively, for which $R_p \sim -0.5$ cm^{-1}/MPa, $f\cdot\Delta\mu \sim 2.4$ D, and $S_t \sim 2.0$.[39,40] The values for P680 and P684 of the isolated PS II RC are ∼ −0.14 cm^{-1}/MPa, ∼0.9 D and 0.9, values that are inconsistent with appreciable electron exchange coupling between the cofactors, in particular P_1 and P_2.

Acknowledgment. Research at the Ames Laboratory was supported by the Division of Chemical Sciences, Office of Basic Energy Sciences, U.S. Department of Energy. Ames Laboratory is operated for USDOE by Iowa State University under Contract W-7405-Eng-82. Authors are thankful to Drs. Tõnu Reinot and John M. Hayes (ISU), Dr. Thomas Renger (Humboldt University, Berlin), Dr. Rafael Picorel (E. E. Aula Dei, Zaragoza), Dr. Michael Seibert (NREL, Golden, Colorado), Drs. Ronald Pace and Elmars Krausz (The Australian National University), and Dr. Valentin Prokhorenko (Max-Planck-Institut für Strahlenchemie, Mülheim a.d. Ruhr) for fruitful discussions.

References and Notes

(1) Nanba, O.; Satoh, K., *Proc. Natl. Acad. Sci. U.S.A.* **1987**, *84*, 109.
(2) Dekker, J. P.; van Grondelle, R. *Photosynth. Res.* **2000**, *63*, 195.
(3) Zouni, A.; Witt, H. T.; Kern, J.; Fromme, P.; Kraub, N.; Saegner, W.; Orth P. *Nature* **2001**, *409*, 739.
(4) Small, G. J. *Chem. Phys.* **1995**, *197*, 239.
(5) Vacha, F.; Joseph, D. M.; Durrant, J. R.; Telfer, A.; Klug, D. R.; Porter, G.; Barber, J. *Proc. Natl. Acad. Sci. U.S.A.* **1995**, *92*, 2929.
(6) Durrant, J. R.; Klug, D. R.; Kwa, S. L. S.; van Grondelle, R.; Porter, G.; Dekker, J. P., *Proc. Natl. Acad. Sci. U.S.A.* **1995**, *92*, 4798.
(7) Svensson, B.; Etchebest, C.; Tuffery, P.; van Kan, P.; Smith, J.; Styring, S. *Biochemistry* **1996**, *35*, 14486.
(8) Tetenkin, V. L.; Gulyaev, B. A.; Seibert, M.; Rubin, A. B. *FEBS Lett.* **1989**, *250*, 459.
(9) Jankowiak, R.; Hayes, J. M.; Small, G. J. *J. Phys. Chem. B* **2002**, *106*, 8803.
(10) Renger, T.; Marcus, R. A. *J. Phys. Chem. B* **2002**, *106*, 1809.
(11) Prokhorenko, V. I.; Holzwarth, A. R. *J. Phys. Chem. B* **2000**, *104*, 11563.
(12) Vasil'ev, S.; Orth, P.; Zouni, A.; Owens, T. G.; Bruce, D. *Proc. Natl. Acad. Sci. U.S.A.* **2001**, *98*, 8602.

(13) Groot, M. L.; van Mourik, F.; Eijckelhoff, C.; van Stokkum, I. H. M.; Dekker, J. P.; van Grondelle, R. *Proc. Natl. Acad. Sci. U.S.A.* **1997**, *94*, 4389.
(14) Wasielewski, M. R.; Johnson, D. G.; Seibert, M.; Govindjee, *Proc. Natl. Acad. Sci. U.S.A.* **1989**, *86*, 524.
(15) Wiederrecht, G. P.; Seibert, M.; Govindjee, Wasielewski, M. R. *Proc. Natl. Acad. Sci. U.S.A.* **1994**, *91*, 8999.
(16) Schelvis, J. P. M.; van Noort, P. I.; Aartsma, T. J.; van Gorkom, H. J. *Biochim. Biophys. Acta* **1994**, *1184*, 242.
(17) Gatzen, G.; Müller, M. G.; Griebenow, K.; Holzwarth, A. R. *J. Phys. Chem.* **1996**, *100*, 7269.
(18) Greenfield, S. R.; Seibert, M.; Govindjee, Wasielewski, M. R. *J. Phys. Chem. B* **1997**, *101*, 2251.
(19) Merry, S. A.; Kamzaki, S.; Tachibana, Y.; Joseph, D. M.; Porter, G.; Yoshohara, K.; Barber, J.; Durrant, J. R.; Klug, D. R. *J. Phys. Chem. B* **1996**, *100*, 10469.
(20) Jankowiak, R.; Tang, D.; Small, G. J.; Seibert, M. *J. Phys. Chem.* **1989**, *93*, 1649.
(21) Tang, D.; Jankowiak, R.; Seibert, M.; Small, G. J. *Photosynth. Res.* **1991**, *27*, 19.
(22) Wasielewski, M. R.; Johnson, D.; Govindjee, Preston, C.; Seibert, M. *Photosynth. Res.* **1989**, *22*, 89.
(23) Visser, H. M.; Groot, M.-L.; van Mourik, F.; van Stokkum, I. H.; Dekker, J. P.; van Grondelle, R. *J. Phys. Chem.* **1995**, *99*, 15304.
(24) Greenfield, S. R.; Seibert, M.; Wasielewski, M. R. *J. Phys. Chem. B* **1999**, *103*, 8364.
(25) Jankowiak, R.; Rätsep, M.; Hayes, J. M.; Zazubovich, V.; Picorel, R.; Seibert, M.; Small, G. J. *J. Phys. Chem. B* **2003**, *107*, 2068.
(26) van Kan, P. J. M.; Otte, S. C. M.; Kleinherenbrink, A. M.; Nieveen, M. C.; Aartsma, T. J.; van Gorkom, H. J. *Biochim. Biophys. Acta* **1990**, *1020*, 146.
(27) Otte, S. C. M.; van der Vos, R.; van Gorkom, H. J. *Photochem. Photobiol. B: Biol.* **1992**, *15*, 5.
(28) Chang, H.-C.; Jankowiak, R.; Reddy, N. R. S.; Yocum, C. F.; Picorel, R.; Seibert, M.; Small, G. J. *J. Phys. Chem.* **1994**, *98*, 7725.
(29) Groot, M. L.; Dekker, J. P.; van Grondelle, R.; den Hartog, F. T. H.; Völker, S. *J. Phys. Chem.* **1996**, *100*, 11488.
(30) den Hartog, F. T. H.; Vacha, F.; Lock, A. J.; Barber, J.; Dekker, J. P.; Völker, S. *J. Phys. Chem. B* **1998**, *102*, 9174.
(31) Peterman, E. J. G.; van Amerongen, H.; van Grondelle, R.; Dekker, J. P. *Proc. Natl. Acad. Sci. U.S.A.* **1998**, *95*, 6128.
(32) Smith, P. J.; Peterson, S.; Masters, V. M.; Wydrzynski, T.; Styrling, S.; Krausz, E.; Pace, R. J. *Biochemistry* **2002**, *41*, 1981.
(33) Reddy, N. R. S.; Picorel, R.; Small, G. J. *J. Phys. Chem.* **1992**, *96*, 6458.
(34) Rätsep, M.; Wu, H.-M.; Hayes, J. M.; Blankenship, R. E.; Cogdell, R. J.; Small, G. J. *J. Phys. Chem*. B **1998**, *102*, 4035.
(35) Chang, H.-C.; Jankowiak, R.; Reddy, N. R. S.; Small, G. J. *Chem. Phys.* **1995**, *197*, 307.
(36) Kwa, S. L. S.; Eijckelhoff, C.; van Grondelle, R.; Dekker, J. P. *J. Phys. Chem.* **1994**, *98*, 7702.
(37) Jankowiak, R.; Rätsep, M.; Picorel, R.; Seibert, M.; Small, G. J. *J. Phys. Chem. B* **1999**, *103*, 9759.
(38) Chang, H.-C.; Small, G. J.; Jankowiak, R. *Chem. Phys.* **1995**, *194*, 323.
(39) Rätsep, M.; Johnson, T. W.; Chitnis, P. R.; Small, G. J. *J. Phys. Chem. B* **2000**, *104*, 836.
(40) Zazubovich, V.; Matsuzaki, S.; Johnson, T. W.; Hayes, J. M.; Chitnis, P. R.; Small, G. J. *Chem. Phys.* **2002**, *275*, 47.
(41) Wu, H.-M.; Rätsep, M.; Young, C. S.; Jankowiak, R.; Blankenship, R. E.; Small, G. J. *Biophys. J.* **2000**, *79*, 1561.
(42) Köhler, M.; Friedrich, J.; Fidy, J. *Biochim. Biophys. Acta* **1998**, *1386*, 255.
(43) Kador, L.; Haarer, D.; Personov, R. *J. Chem. Phys*. **1987**, *86*, 5300.
(44) Lyle, P. A.; Kolaczkowski, S. V.; Small, G. J. *J. Phys. Chem*. **1993**, *97*, 6924.
(45) Hayes, J. M.; Lyle, P. A.; Small, G. J. *J. Phys. Chem*. **1994**, *98*, 7337.
(46) Matsuzaki, S.; Zazubovich, V.; Rätsep, M.; Hayes, J. M.; Small, G. J. *J. Phys. Chem. B* **2000**, *104*, 9564.
(47) Lee, I.-J.; Small, G. J. *J. Phys. Chem.* **1990**, *94*, 3376.
(48) Reddy, N. R. S.; Kolaczkowski, S. V.; Small, G. J. *J. Phys. Chem*. **1993**, *97*, 6934.
(49) Hillmann, B.; Brettel, K.; van Mieghem, F., Kamlowski, A.; Rutherford, A. W.; Schlodder, E. *Biochemistry* **1995**, *34*, 4814.
(50) Vink, K. J.; de Boer, S.; Plijter, J. J.; Hoff, A. J.; Wiersma, D. A. *Chem. Phys. Lett*. **1987**, *142*, 433.
(51) Reinot, T.; Small, G. J. *J. Chem. Phys*. **2000**, *113*, 10207.
(52) Groot, M.-L.; Peterman, E. J. G.; van Kan, P. J. M.; van Stokkum, I. H. M.; Dekker, J. P.; van Grondelle, R. *Biophys. J.* **1994**, *67*, 318.
(53) Völker, S. *J. Lumin.* **1987**, *36*, 251.
(54) van der Zaag, P. J.; Galaup., J. P.; Völker, S. *Chem. Phys. Lett.* **1990**, *174*, 467.
(55) Pieper, J.; Voigt, J.; Renger, G.; Small, G. J. *Chem. Phys. Lett*. **1999**, *310*, 296.
(56) Frese, R. N.; Germano, M.; de Weerd, F. L.; van Stokkum, I. H. M.; Shkuropatov, A. Y.; Shuvalov, V. A.; van Gorkom, H. J.; van Grondelle, R.; Dekker, J. P. *Biochemistry* **2003**, *42*, 9205.
(57) Kamiya, N.; Shen, J.-R. *Proc. Natl. Acad. Sci. U.S.A.* **2003**, *100*, 98.
(58) Diner, B.; Rappaport, F. *Annu. Rev. Plant Biol.* **2002**, *53*, 551.
(59) Reinot, T.; Zazubovich, V.; Hayes, J. M.; Small, G. J. *J. Phys. Chem. B* **2001**, *105*, 5083.